

Accelerator Simulation Activities at the SSCL

G. Bourianoff

Superconducting Super Collider Laboratory*
2550 Beckleymeade Ave.
Dallas, TX 75237

January 1993

*Operated by the Universities Research Association, Inc., for the U.S. Department of Energy under Contract No. DE-AC35-89ER40486.

Accelerator Simulation Activities at the SSCL

by
George Bourianoff SSCL

Introduction

This paper will attempt to summarize the activities related to accelerator simulation at the SSC laboratory during the recent past. The work presented here will largely be the work of others and specific contributors are identified in the acknowledgments. The majority of the work was done by the Machine Simulation and Correction Group with contributions from individual machine groups and the Accelerator Theory Group.

The paper will be organized into three basic areas as follows. The first section deals with operational simulations. As the name implies, the results presented here deal with simulating various routine accelerator operations such as injection, extraction and correction. The topic or correction includes many specific operations such as chromatic correction, decoupling, and orbit smoothing as well as corrector failure simulations. Specific examples that will be discussed here are local chromatic correction of the low beta insertion of the collider, experimental determination of local coupling strengths in LEP, and results of steering corrector failure simulations in the collider.

The second section deals with performance prediction of a specified lattice design. This involves running the tracking kernel of the code to evaluate the performance of a specific configuration. This is usually done as part of a family of runs to investigate parametric dependencies by incrementally changing one parameter and observing the results. The effects are usually quantified by either the linear aperture or dynamic aperture. The specific results to be discussed here include the effect of higher order multipoles on linear aperture and the effect of power supply ripple on emittance growth in the collider.

The third area discusses development and application of advanced techniques to particle tracking. The goal is to extend the scope of problems that may be attacked with tracking codes beyond the current range. One approach is to apply the computational power of the current generation of parallel processors to accelerator physics simulation, while the other technique is to utilize high order maps to extend the range of simulations. Both approaches are being exploited at the SSC. The recent developments in parallel processing will be described here and mapping techniques are discussed separately in a paper by Yiton Yan in these proceedings.

Operational Simulation

LOCAL CHROMATICITY CORRECTIONS

The first example of operational simulation to be described here is described more fully in Ref. [1] in this proceedings. It discusses the local chromatic corrections made to correct for the effect of the strong focusing quadrupoles in the low beta insertion and the simulations done to support that effort.

The natural chromaticity of the collider is approximately -170 units of chromaticity from the arcs. For β^* equal to 0.5 m, each IR contributes an additional -50 units of chromaticity and

correspondingly -100 units for β^* of 0.25 m. The current design calls for 4 families of sextupole correctors located adjacent to the IR regions to be used to correct part or all of the IR induced chromaticity. The simulations described here were used to quantitatively evaluate the relative performance of the different operational scenarios that were possible with the available set of sextupoles.

The simulation effort required evaluating a three dimensional array of parameters and therefore consisted of a great number of individual cases. The possible optics configurations of the low beta IRs are shown in Table 1. These 6 cases constitute one of the three dimensions mentioned above.

Case	β_n^*	β_s^*
I	0.25 m	0.25 m
II	0.25 m	0.50 m
IV	0.25 m	8.00 m
V	0.50 m	0.50 m
VII	0.50 m	8.00 m
X	8.00 m	8.00 m

Table 1: Optics Configurations Studied

The second dimension of this three dimensional parameter space specifies the amount of chromaticity corrected by the local correction scheme with the remaining chromaticity corrected by the global scheme. For example, the curves labeled *local 50 + 50* indicate that 50 units of chromaticity are compensated by each of the local corrector families. The curves marked *local 0+0* do not use the local correctors to correct any first order chromaticity but use them to balance the chromatic contributions of the two IRs when they are operated asymmetrically. A full discussion and analysis of this situation is contained in Ref[1].

The last dimension of the parameter space defines the distribution of errors in the lattice. The local chromatic correction scheme requires precise phase relationships between the various members of a correction family and hence is sensitive to the magnitude and distribution of errors in the lattice. The dynamic aperture calculations were done with various combinations of errors in the arcs and IR regions to study this dependence.

The results of this study are summarized in Figures 1 to 4. These show the 1000 turn dynamic aperture as a function of betatron amplitude and momentum offset. This set of curves displays only one of the six optics configurations (0.25m+8.00m). The other cases were calculated but are not shown here. The curves show that the local schemes have a larger momentum aperture relative to the globally corrected case.

The brief summary of this work given here is meant only to give an overview of the scope and content of the effort. A complete analysis and discussion are contained in Ref[1].

n25s800: ideal lattice

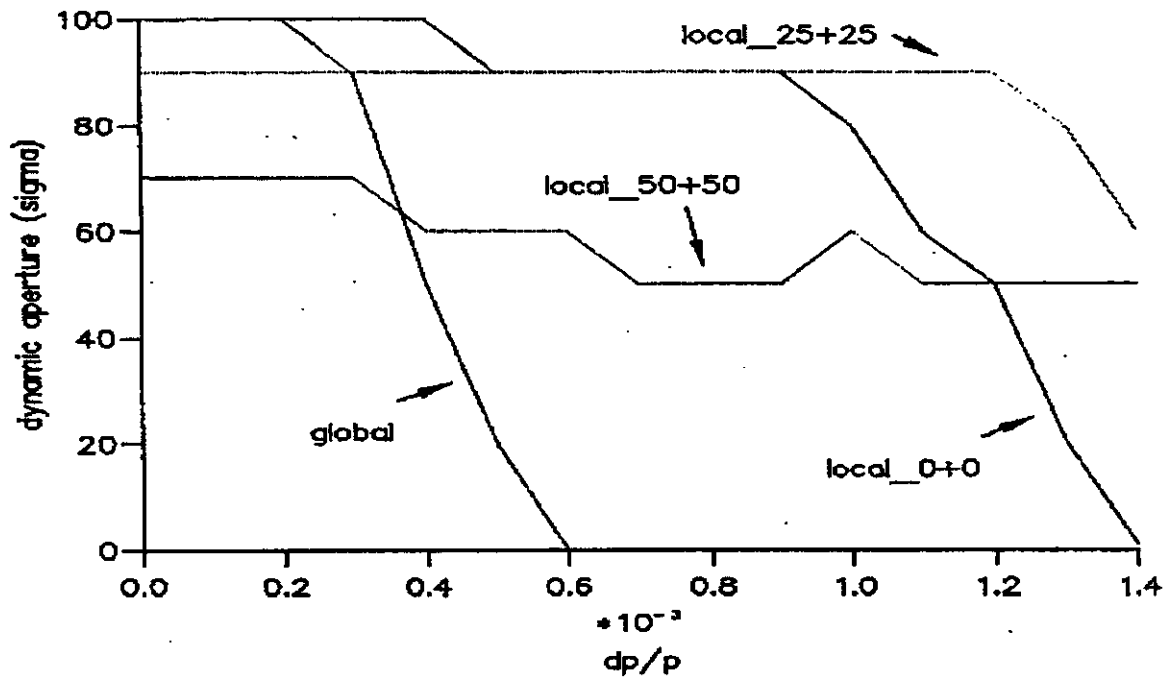


Figure 1. Dynamic Aperture as a Function of Amplitude and Momentum

n25s800: field errors in the arcs

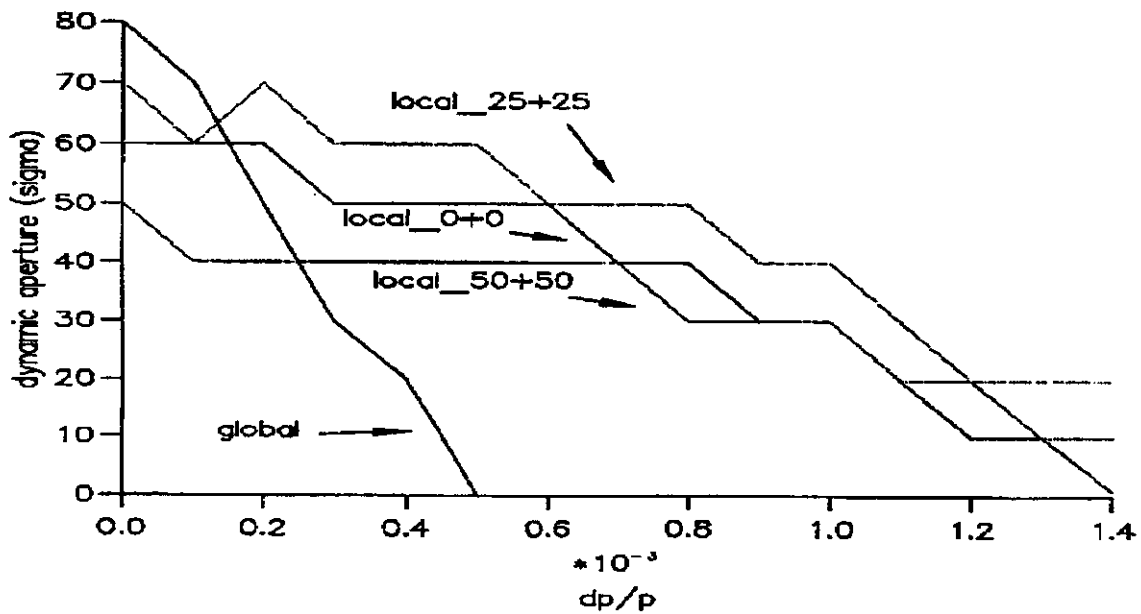


Figure 2. Dynamic Aperture as a Function of Amplitude and Momentum

n25s800: field errs in arc and irs

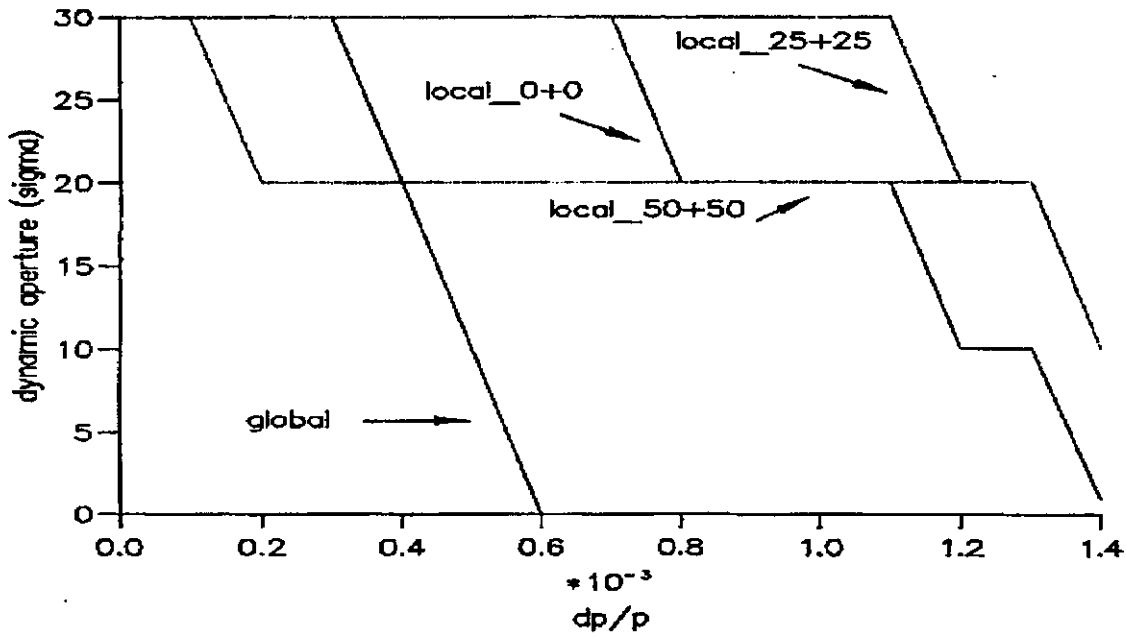


Figure 3. Dynamic Aperture as a Function of Amplitude and Momentum

n25s800: field errs in arc, irs, triplets

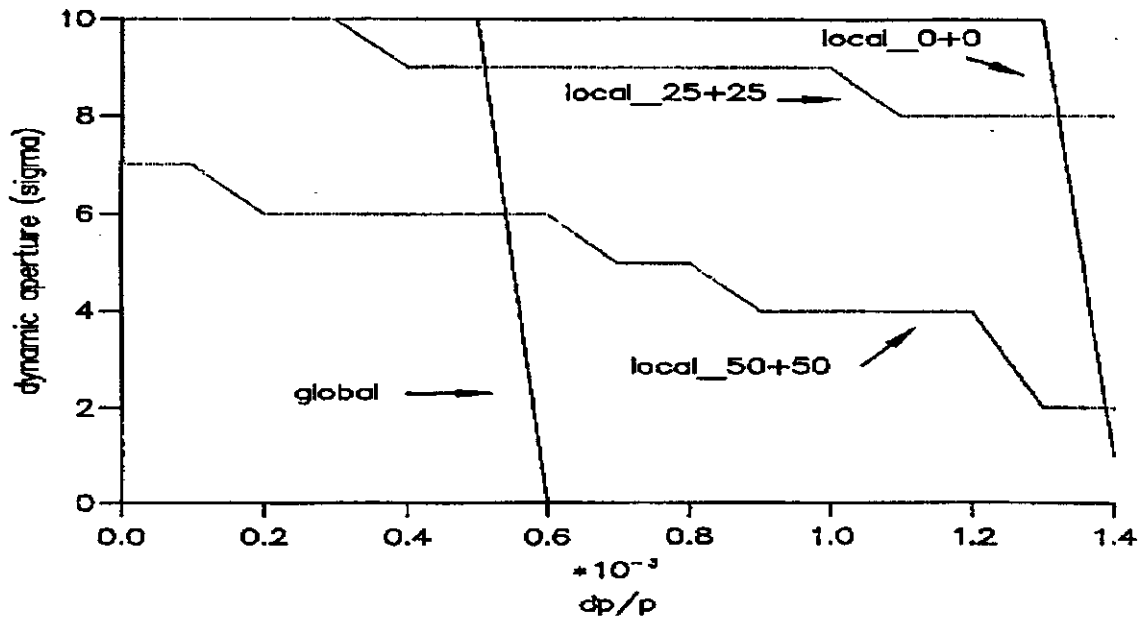


Figure 4. Dynamic Aperture as a Function of Amplitude and Momentum

COUPLING MEASUREMENTS AT LEP

A second example of operational simulations could equally well be discussed under the second section of this report dealing with performance prediction since it deals with both topics. The example to be discussed is the measurement of local coupling coefficients at LEP by analyzing turn by turn BPM data and comparing the measured results to simulation results. The motivation for this effort is that the random skew quadrupole component of the SSC dipoles will cause the betatron motion to be strongly coupled and interfere with routine accelerator operations. Standard techniques of decoupling using the closest tune approach will not be able to control the deviations of the eigenplanes in the arc and it is therefore necessary to detect and correct the coupling locally.

The theoretical foundation for this procedure is contained in Ref.[2]. However, there existed operational questions about ones ability to measure the needed parameters to the required accuracy in an operational environment. The description of the experimental procedures, signal processing, supporting simulations and measured results are summarized here and more fully described in Ref.[3].

The basic formalism for local decoupling contained in Ref.[2] is summarized here for the sake of completeness. The basic goal is to block diagonalize the once-around transfer matrix M.

$$M = \begin{bmatrix} A & B \\ C & D \end{bmatrix} \quad (1)$$

where A, B, C, and D are all 2X2 submatrices. It has been shown in Ref[3] that M may be diagonalized by the transformation.

$$\begin{bmatrix} \overline{A} & 0 \\ 0 & \overline{D} \end{bmatrix} = g^2 \begin{bmatrix} I & -R_D \\ -R_A & I \end{bmatrix} \begin{bmatrix} A & B \\ C & D \end{bmatrix} \begin{bmatrix} I & -R_D \\ -R_A & I \end{bmatrix} \quad (2)$$

where symplectic conjugation is indicated by an overbar and

$$R_A = \frac{C + \overline{B}}{\Lambda_A - trD} \quad R_D = \frac{B + \overline{C}}{\Lambda_D - trA} \quad (3)$$

$$\Lambda_{A,D} = \left(\frac{trA + trD}{2} \right) \pm \sqrt{\frac{(trA - trD)^2}{4} + det|C + \overline{B}|}$$

$$g^2 = \frac{|\Lambda_D - trA|}{|\Lambda_D - \Lambda_A|} \quad \Lambda_{A,D} = 2 \cos(\mu_{A,D}) \quad (4)$$

Λ_A and Λ_D , the eigenvalues of the matrix $M + \overline{M}$, are related to the generalized betatron tunes μ_A and μ_D as shown above. In what follows, the nominally horizontal (vertical) motion will be labeled A (D).

At a fixed point in the lattice of a coupled machine, the A betatron oscillations will be visible in the y motion and the D oscillations will be visible in x. The A betatron motion may be readily distinguished from the D betatron motion on the basis of their characteristic frequencies. The x and y motion at a fixed point and at the A betatron frequency may be written

$$\begin{aligned} x &= g \cos(-\Psi_A) \\ y &= g e_A \cos(-\Psi_A + \Phi_A) \end{aligned}$$

where

$$\begin{aligned} e_A^2 &= \left[R_{A11} + \left(\frac{\alpha_A}{\beta_A} R_{A12} \right) \right]^2 + \left(\frac{R_{A12}}{\beta_A} \right)^2 \\ \Phi_A &= -\text{atan} \left(\frac{R_{A12}/\beta_A}{R_{A11} - (\alpha_A/\beta_A) R_{A12}} \right) \end{aligned} \quad (5)$$

where Ψ_A is the phase advance per turn of the A betatron motion. It can be seen from Eq. 5 that two constants e_A and Φ_A define the state of local coupling from x to y at a given location in the lattice. Two additional constants could be defined in order to parameterize the coupling from y to x but it will be assumed here that this coupling is essentially reciprocal since the eigenplanes are approximately (but not exactly) perpendicular. Further discussion of this is contained in the accompanying Ref.[3].

The experimental procedure called for a betatron signal to be generated in the horizontal plane with the injection kickers. The constants e_A and Φ_A were determined by Fourier analyzing the X and Y motion at each BPM. The Fourier transforms of the applied signals may be written as.

$$\{X\}_k = \frac{1}{\sqrt{N}} \left(\sum_{j=0}^{N-1} X_j \exp(-i \frac{2\pi j k}{N}) \right) \quad (6)$$

where

$\{X\}$ = Discrete Fourier transform of X

N = Number of discrete time samples (turns)

X_j = Output of Horizontal BPM at turn j

Let the index k_{xmax} be defined to be the k value at which the maximum magnitude of $\{X\}$ occurs. The noise is defined to be the average value of all Fourier components with the exclusion of $k = k_{max}$. The signal to noise ratio of the actual data obtained at LEP is quite good, with 99 per cent lying above 10.0.

The complex function $\{X\}_k$ is converted to polar form

$$\{X\}_k = \rho_{x_k} e^{i\phi_{x_k}} \quad (7)$$

$$e_A = \frac{\rho_{x_{k_{xmax}}}}{\rho_{y_{k_{xmax}}}} \quad \Phi_A = \phi_{x_{k_{xmax}}} - \phi_{y_{k_{xmax}}}$$

and the amplitude ratio ϵ_A and phase difference Φ_A are extracted at every BPM. These are the two pieces of information necessary to perform the decoupling calculation based on experimental data and referenced in Eq. 5. The actual matrix elements needed for computing the corrector strengths (R_{A11} and R_{A12}) are obtained by inverting Eq. 5.

$$R_{A12} = e_A^2 \beta_A \sin(\Phi_A) \quad (8)$$

$$R_{A11} = e_A^2 \cos(\Phi_A) + \frac{\alpha_A}{\beta_A} R_{A12}$$

The experimental effort consisted of measuring the local coupling parameters and comparing them to simulated values determined from a computational model of LEP. The experimentally measured results are shown in Figures 5 and 6.

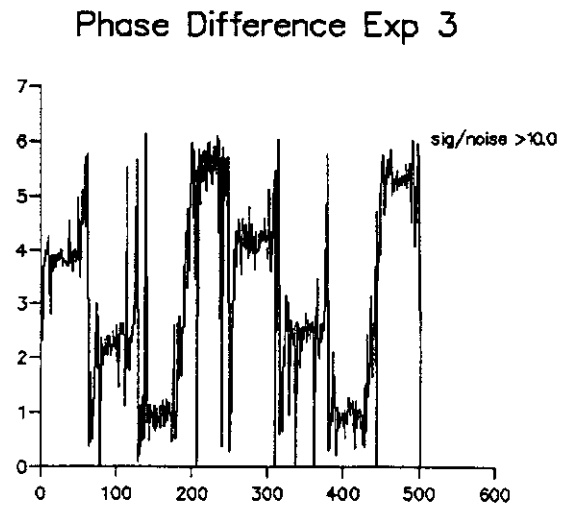
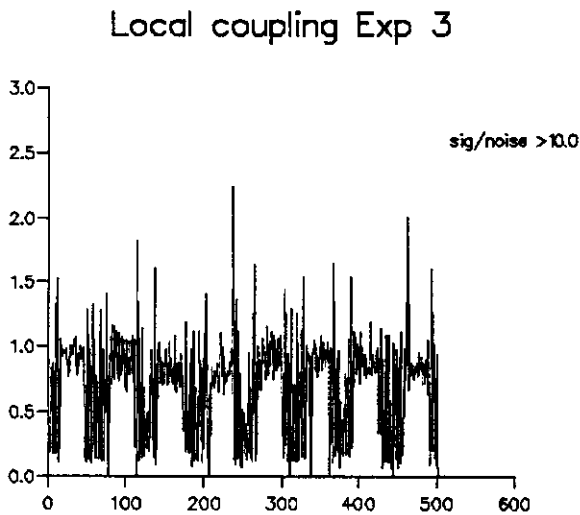


Figure 5. Measured Coupling Coefficient

Figure 6. Measured phase factors

The notation of experiment 3 in these figures distinguishes them from other data in which

the betatron oscillations were generated by methods different from firing the injection kickers. The functions in the graphs are the amplitude ratio ϵ_A and phase difference Φ_A defined in Eq. 7.

This situation was simulated using the teapot simulation code modified to produce an output file identical in structure to the output of the Beam Orbit Measurement system of the real experiment. This data was processed in the same fashion and by the same code and used to produce the plots in Figures 5 and 6. The actual experimental field and alignment errors that contribute to the experimentally measured coupling are of course unknown. The simulation code uses a Monte Carlo algorithm to generate an error distribution with what are believed to be the correct statistical averages (Ref.[4]). In this case, the coupling is produced by a small systematic a_1 component of 0.01 units in the arc dipoles and a random rotation of 2 mrad in the main arc quads; the latter is dominant.

The simulated local coupling coefficients are shown in Figures 7 and 8. A direct comparison of these two figures with Figures 5 and 6 (experimental data) indicates that the coupling characteristics of the simulation agree closely with the coupling characteristics of the experiment. The simulation data is a little "cleaner" than the real data and the peak coupling values in the IR's is approximately 50 percent larger in the experimental case. However, the coupling in the arcs is within 20 percent of the experimental case. Overall, the agreement between experiment and simulation is quite good and we may use it as a base case on which to apply the local decoupling algorithm to estimate its effectiveness. This direct comparison of simulated results to measured results also serves to verify the simulation code in its treatment of basic optics and the treatment of error sources which create the need for operational correction.

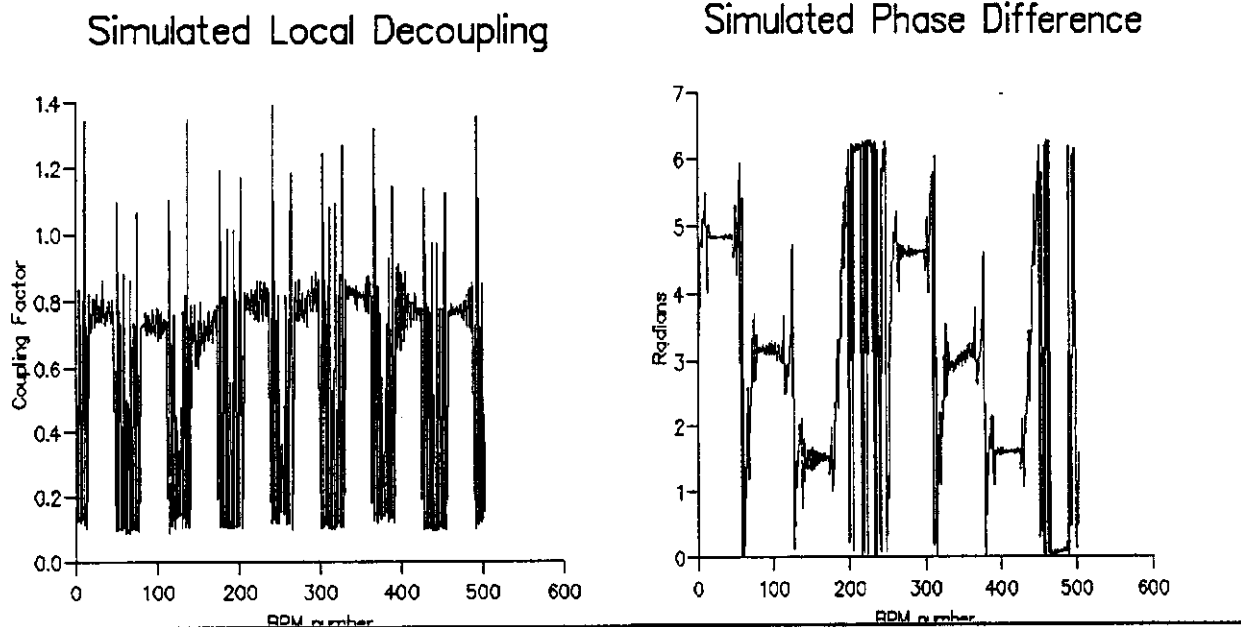


Figure 7 Simulation of Experiment 3

Figure 8 Simulation of Experiment 3

CORRECTOR FAILURE SIMULATIONS

A third example of operational issues that are being addressed through simulation is the impact of the failure of one or more steering correctors on collider operation. Each ring of the collider will contain approximately 1000 independently powered steering correctors. The specified mean time to failure of one of the thousand corrector power supplies is 29 hours. The question addressed in this study is what is the probability that failure of one corrector will cause beam loss or significant degradation of the beam. Beam loss will probably result in quenching of one or more superconducting magnets, resulting in a down time of perhaps half a day.

The simulations used the working collider lattice as of Aug 11. This lattice had all assigned errors (alignment errors, random and systematic field errors) as specified in the Level 3B Specifications. It also used the full set of correctors as specified including 44 skew quadrupoles to correct the coupling. The study was done at collision energy (20 TeV) with tunes of 123.285 for ν_x and 122.265 for ν_y . The distributions of horizontal and vertical strengths steering corrector strengths for this case are shown in Figures 9 and 10. The corrector strengths have a roughly normal distribution with peak values of 1.83 and 2.49 Tesla-meters for the horizontal and vertical cases respectively.

Distribution of Horizontal Corrector Strengths

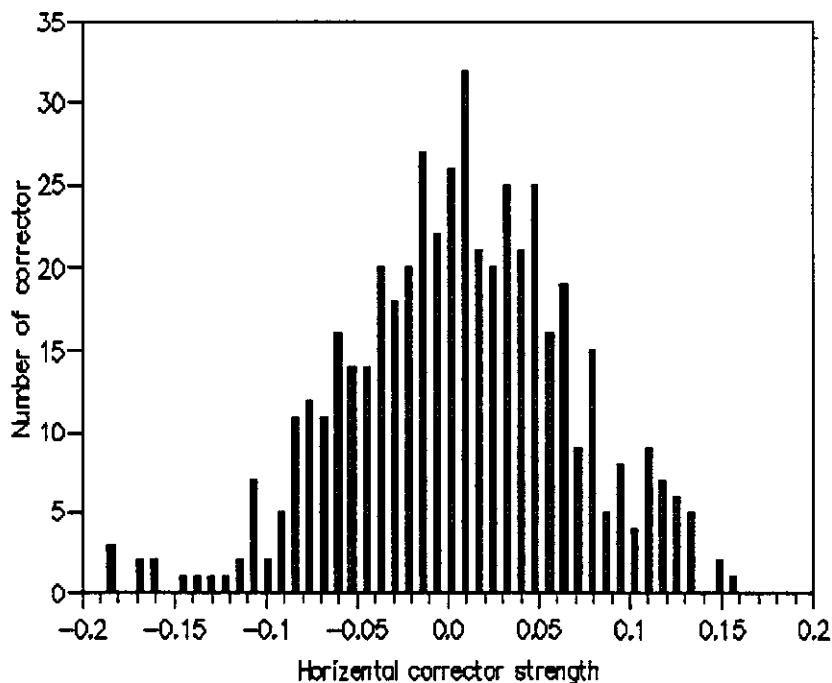


Figure 9. Strength x 0.1 in Tesla-meters

The simulation was done by successively “turning off” correctors beginning at the strongest and proceeding to less strongly powered correctors. Turning off the strongest correctors has the strongest effect. The correctors are grouped in blocks of 10 for this study so the simulations

Distribution of Vertical Corrector Strengths

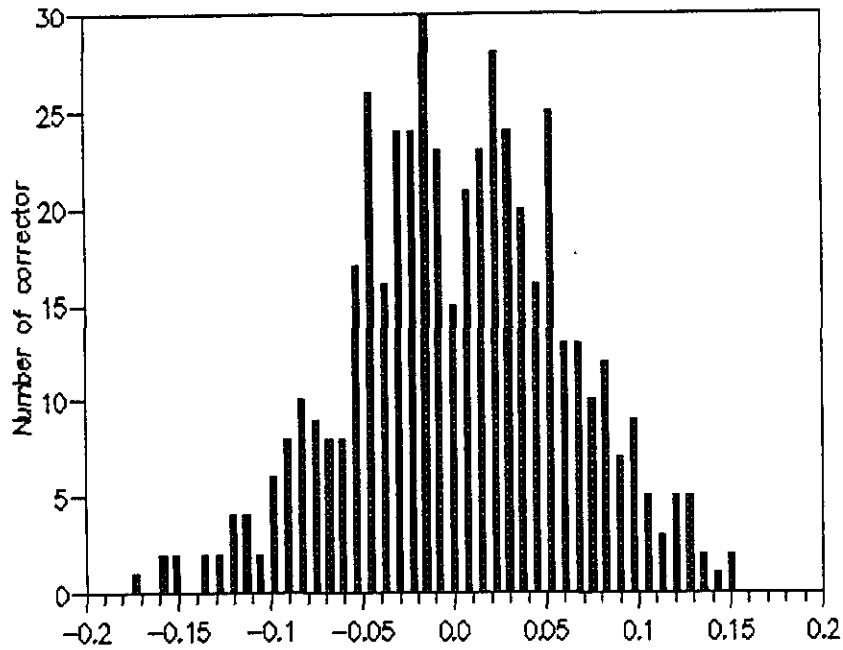


Figure 10. Strength x 0.1 in Tesla-meters

are done by turning off the 11th strongest, 21st strongest, ect.

The results of this process are given in Table 2 in tabular form. The top row of Table 2 gives the standard deviation of the closed orbit, the maximum excursion of the closed orbit and the linear aperture for the reference case (the case where all correctors are functioning).

The study was done for both on momentum and off momentum particles as indicated by the last two columns in Table 2. These columns contain entries of "all," "yes" or "no" for particles lost. The entry "yes" means that some but not all the particles were lost and is further quantified in Figure 11.

The figure shows the relationship of corrector strength to the minimum betatron amplitude at which particles are lost. The corrector strength is specified by rank in the distribution of strengths and is on the vertical axis. The betatron amplitude is expressed in terms of beam spot size ($1\sigma = 0.144\text{mm}$). From this graph, it is possible to determine what fraction of the correctors will effect the core of the beam (arbitrarily defined here to be made up of those particles with betatron amplitude less than 3σ). It can be seen from Fig. 11 that if any of the strongest 20 percent of correctors fail, particles will be lost in the core of the beam. Since there are 470 correctors, the 20th percentile ranking corresponds to the 47th corrector. From table 2, it can be seen that failure of this corrector will produce a rms closed orbit distortion of 2.5mm and a peak closed orbit deviation of 12.0mm.

case	$\sigma_{co}(y)$	Max (y_{co})	Linear Aperture	Particle lost ($dp=0.0$)	Particle lost ($dp=0.0005$)
Reference case	0.1137mm	0.5187mm	0.917mm	No	No
1st				All	All
11th				All	All
21th				All	All
31th	2.201mm	15.49mm		Yes	Yes
41th	1.947mm	13.62mm	0.148mm	Yes	Yes
51th	2.544mm	12.21mm		Yes	Yes
61th	1.73mm	11.86mm	0.17mm	Yes	Yes
71th	1.67mm	9.80mm	0.43mm	Yes	Yes
81th	1.50mm	9.85mm	0.61mm	Yes	Yes
91th	1.42mm	9.48mm	0.81mm	Yes	Yes
100th	1.097mm	7.55mm	0.73mm	No	No

Table 2: Effect of Corrector Failure

The functional dependence shown in figure 11 is characterized by a pronounced dip which makes the function non single valued for certain values of the corrector strength. This may be explained by taking into account the beta function at the corrector location. It turns out that the strength of the correctors is correlated with the local beta function by the optical properties of the lattice. If one defines a parameter called effective strength equal to the corrector strength times the square root of beta, the functional relationship can be displayed as in Fig 12. It can be noticed that a peak in the curve occurs at the 80th percentile which is correlated to the observed dip in Fig. 11

The lost particle amplitude may now be plotted against effective strength as shown in Figure 13. The effective strength corresponding to the top 20 percent of the correctors is indicated and clearly corresponds to the 3σ point. Using effective strength as an independent coordinate eliminates the double valued nature of the function shown in Figure 11.

The figures and discussion here pertain to the vertical motion of the Aug 11 lattice. The analysis has been repeated for the horizontal motion in this lattice and the entire process repeated for two other lattice configurations. The basic result is that there is a 20 percent chance that the failure of 1 corrector will result in loss of all or a significant fraction of the beam. This means that (given the 29 hour MTF) approximately once a week, the beam will be lost due to corrector failure. This is unacceptable and indicates that corrector reliability must be improved.

Vertical corrector percentage vs Amplitude of lost particle

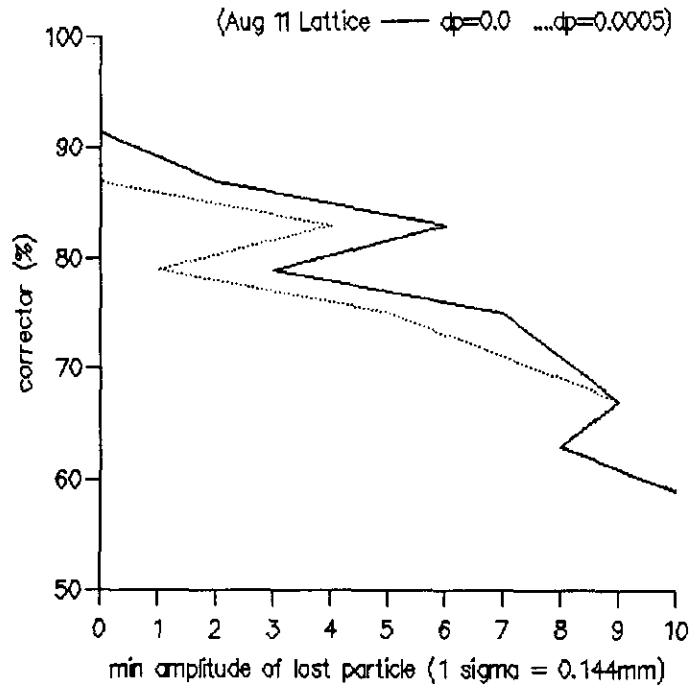


Figure 11. Corrector strength vs. lost particle amplitude

Effective strength vs corrector percentage
(Aug 11 Lattice)

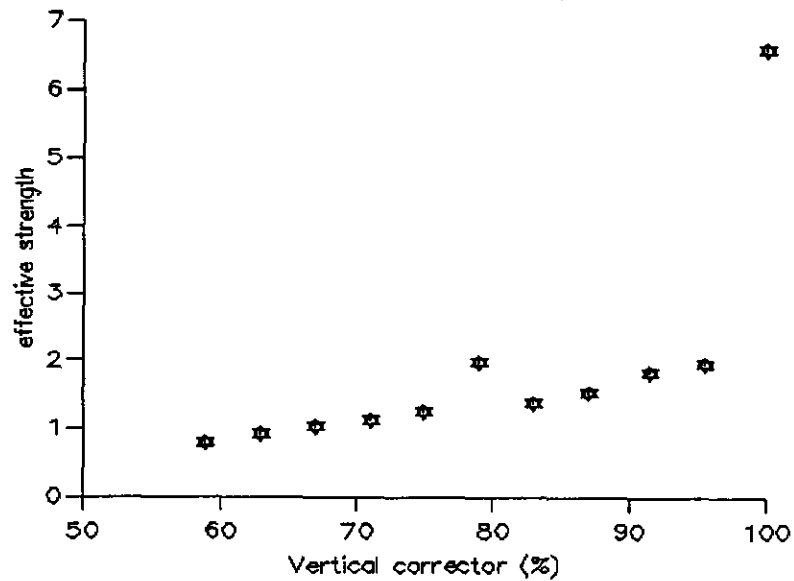


Figure 12. Effective strength vs. corrector ranking

Effective strength vs Amplitude of lost particle
(Aug 11 Lattice for $dp=0.0005$)

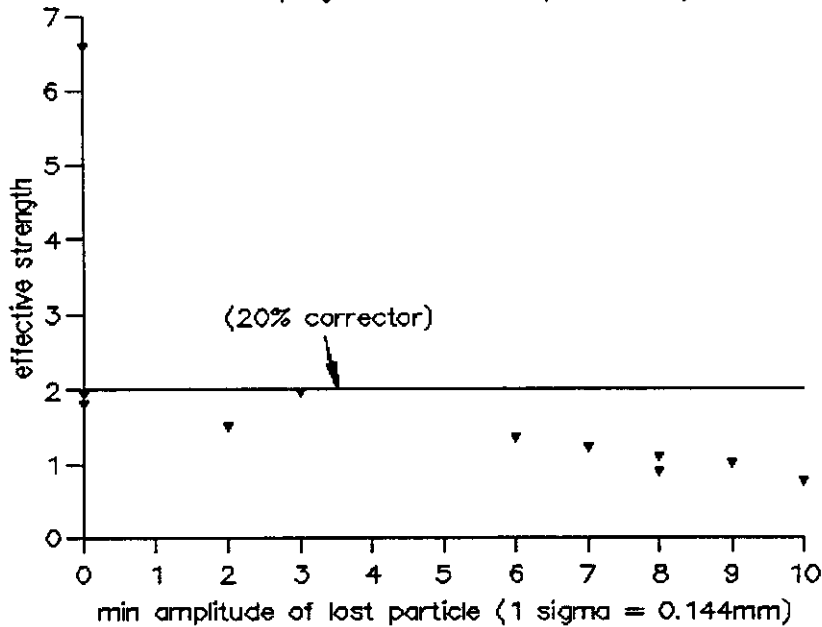


Figure 13 Effective strengths vs. lost particle amplitude

Performance Prediction

The second major area of activity is performance prediction. As the name implies, this activity will simulate the performance of a given lattice configuration, normally comparing the performance of a family of lattices differing only in one parameter. The simulation does not in general require any of the correction capabilities built into the TEAPOT code described in reference 5 and can be done using only the tracking kernel of TEAPOT on a parallel processor or other mainframe computer. These simulations tend to be much more computationally intensive than the simulations described in the first section because a set of lattices must be tracked for a sufficient number of random seeds for a sufficient number of turns. As an example, the calculation of the effect of higher order multipoles on collider performance required ten seeds for five cases to generate the required statistics. Each run required approximately 20 hours on an HP70 RISC station leading to a total 1000 hours of computation on a high performance workstation array.

HIGHER ORDER MULTIPOLES

The first example to be discussed is the impact of higher order multipoles on collider performance. The problem is framed in terms of calculating the linear aperture for 5 separate cases which correspond to the HOM levels exceeding the level 3B specifications by factors of 2 or 4. The specified levels of random and systematic field errors for the dipoles magnets in the collider

are contained in the level 3b specifications and shown in Table 3. The strengths in the table are

Order	Systematic a_n	Systematic b_n	Random a_n	Random b_n
1	0.04	0.04	1.25	0.50
2	0.032	-2.0	0.35	1.15
3	0.026	0.026	0.32	0.16
4	0.02	0.08	0.05	0.22
5	0.016	0.016	0.05	0.02
6	0.013	0.02	0.01	0.02
7	0.01	0.01	0.01	0.01
8	0.008	0.02	0.0075	0.0075

Table 3: Specified Higher Order Multipole Strengths

Tesla times 10^{-4} measured at 1 cm.

The simulation consisted of increasing the values of systematic b_3 and b_4 by factors of 2 and ten relative to the entries in the table. The lattice used was the Mar31 lattice with tunes of 123.765 and 122.2791 for ν_x and ν_y respectively. Two sets of 17 particles were loaded with initial betatron amplitudes ranging from 0.4mm to 8.4mm (1σ - 21σ). The two sets had different momenta with one set being on momentum and the other having a $\delta p/p$ of 0.0005. The particles were tracked for 1024 turns and tune versus amplitude plots such as shown in figure 14 were produced for each set of particles.

TUNE VERSUS AMPLITUDE

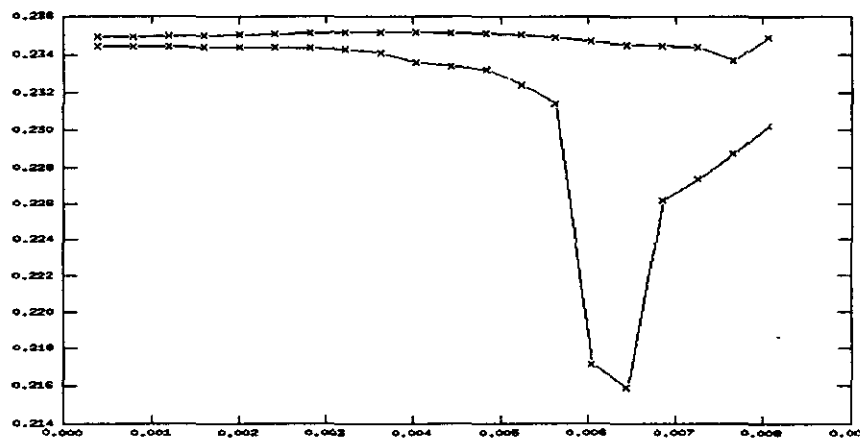


Figure 14. Horizontal tune versus amplitude for Oct X 2 case

The linear apertures for the 5 cases based on 10 random seeds each were computed. The

results for one case is shown in table 4.

seed	$\delta v_x < .005$	$\delta v_y < .005$	smear <5% @ $\delta p = 0.0$	smear <5% @ $\delta p = .0005$	Linear Aperture
1015	7.7 mm	5.8 mm	6.86 mm	6.86 mm	5.8 mm
2701					
3455	7.7 mm	5.8 mm	6.05 mm	5.65 mm	5.65 mm
4011	7.6 mm	6.3 mm	1.6 mm	2.8 mm	1.6 mm
5176	6.1 mm	5.1 mm	5.65 mm	5.24 mm	5.1 mm
6869	6.5 mm	5.6 mm	5.24 mm	5.24 mm	5.24 mm
7531	7.3 mm	6.1 mm	6.45 mm	6.05 mm	6.05 mm
8999	7.7 mm	6.4 mm	6.45 mm	7.26 mm	6.4 mm
9204	>8.0 mm	6.0 mm	5.65 mm	2.82 mm	2.82 mm
10975	> 8.0 mm	6.1 mm	6.86 mm	6.05 mm	6.05 mm
MEAN	7.4 mm	5.9 mm	5.64 mm	5.33 mm	4.96 mm
STD DEV	0.66 mm	0.39 mm	1.61 mm	1.57 mm	1.64 mm

Table 4: Octupole X 2 Case

The smear is loosely defined to be the turn to turn variation of a quantity proportional to the linear invariant expressed as a percentage (an exact quantitative definition can be found in Ref.[6]). It is therefore a measure of the nonlinearity of the motion and is hence an increasing function of amplitude. The entry in the table defines the radius at which the smear exceeds 5 percent which is somewhat arbitrarily defined as the point at which nonlinearity limits machine performance. The linear aperture is defined to be the smallest of the 4 radii shown in table 4. A mean and standard deviation for the 10 seeds is computed for each of the 5 cases studied.

The results, shown in Figure 15, indicate that the machine performance as quantified by the linear aperture would not be affected if the dipole magnets exceeding the specifications by a factor of 10 in the decapole component and a factor of 2 in the octupole component.

A similar calculation was performed to assess the impact of b_5 and b_9 components in all quadrupoles and separately in the triplet quads located in the low beta insertions. The emphasis on b_5 and b_9 is due to two factors, the first being that they are by far the largest of the multipole components and the second being that they are "allowed" multipoles and can in principle be improved by rearranging conductors.

This set of simulations was carried out on a lattice that includes closed orbit steering dipoles in the IR region that produce a crossing angle of 135 μ rad. This is relevant to the present simulation since the non zero crossing angle will cause the beam to traverse the triplet quads off axis and therefore see stronger nonlinear fields, adversely affecting the dynamic aperture.

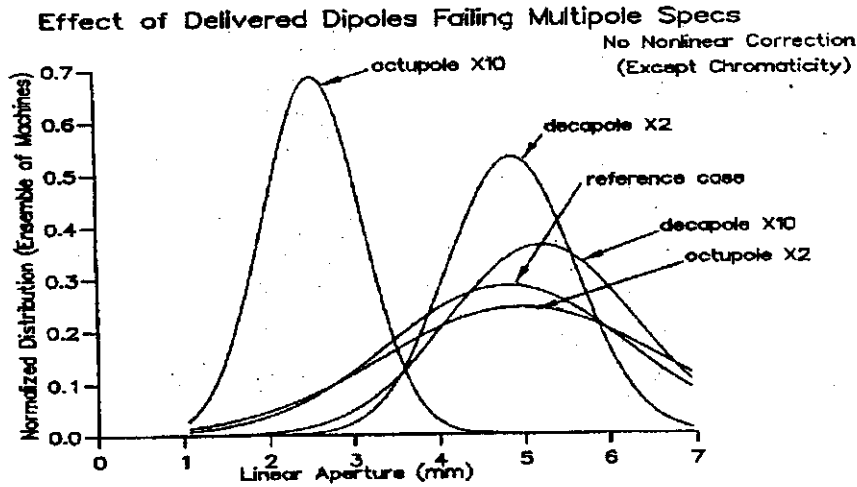


Figure 15. Linear Aperture Distributions

Table 5 shows the dependence of short term dynamic aperture on the presence or absence of b_5 in different sets of quadrupoles.

systematic b_5	$\delta p/p = 0$	$\delta p/p = 10^{-4}$	$\delta p/p = 4 \cdot 10^{-4}$
$b_5 = 1.4(0.573)$ in all 4(5)cm quads	9	10	9
$b_5 = 0$ in triplets	12	12	12
$b_5 = 0$ in triplets and 5cm quads	12	12	11
$b_5 = 0$ in all quads	12	12	11

Table 5: Effect of b_5

The representation in Table 5 is based on classifying all quadrupoles into 1 of 3 groups. There are 4 cm arc quads, 5 cm tuning quads in the IR regions and 5 cm triplet quads in the IR region. The first row has b_5 in all quads at the specified level. By comparing the first and second row of Table 5 to the other rows, it may be deduced that the b_5 component in the triplet quads has the 3σ impact on the dynamic aperture. Comparing the other rows shows that the b_5 component is insignificant in the other quadrupoles.

The impact of b_5 in the triplet may be further quantized by varying this parameter incrementally between 0.0 and the specified value of 0.574 and look for existence of a threshold. The results of this investigation are shown in Table 6. The value of b_9 was set to zero for the purposes of this study. The table reveals a threshold at a b_5 value of about 0.3 units. The existence of such nonlinear thresholds is not surprising but their exact location in parameter space is in general not known and their mapping constitutes one of the most important results of computer simulation of nonlinear systems.

The fact that the linear aperture goes to zero in some cases above is indicative of resonance

sys b_5	dynamic aperture	linear aperture	dynamic aperture	linear aperture	dynamic aperture	linear aperture
(triplets)	$dp/p=0$	$dp/p=0$	$dp/p=10^{-4}$	$dp/p=10^{-4}$	$\delta p/p=4 * 10^{-4}$	$\delta p/p=4 * 10^{-4}$
0.	14	4	12	5	13	0
0.1	14	4	14	4	12	0
0.2	13	4	12	4	11	0
0.3	13	4	11	4	11	0
0.4	11	3	11	4	11	0
0.574	11	3	11	4	10	0

Table 6: Effect of varying b_5 in the triplet quadrupoles

behavior and could probably be remedied by shifting the tune slightly. This remains to be demonstrated.

RIPPLE

A second important example of performance prediction deals with the calculation of the effect of power supply ripple on beam emittance. This is a very difficult problem to simulate directly because very small effects accumulate over very long times in a very nonlinear system.

There are 10 power feed points in each main collider ring at which power is transmitted from the surface to the ring. The superconducting dipoles and quadrupoles are connected as a series string on superconducting buses. These components all have inductance, capacitance and resistance and form a transmission line impedance to the propagation of the AC current components (the ripple). The detailed analysis of this transmission line will not be described here but the results of that analysis have been included in the performance prediction as follows.

The strongest AC ripple components of the dipole *magnetic* field expressed in terms of $\delta B/B$ is shown in Table 7 as a function of frequency.

The ripple amplitudes are given at injection energy field amplitudes and collision energy field amplitudes. The field amplitudes are exponentially damped as a function of distance from the feedpoint. The exponential damping length expressed in units of cell lengths is given in the fourth column of table 7. The column marked relative influence is simply the product of decay length by the amplitude (at injection energy) normalized to the most influential frequency. The frequency sensitivity of the particle motion in the accelerator has not been included in this numerical factor.

The ripple simulation was done using a superposition of components at 4 frequencies at 120, 720, 1440 and 2880 hz. These frequencies were selected by considerations of beam dynamics. The number of frequencies was limited to 4 by the memory available on the Intel ISPC/860 parallel computer where the calculations were performed.

Freq. hz	Injection $\delta B/B$	Collision $\delta B/B$	Decay Length-cells	Rel. Influence
60	1.00e-7	2.76e-8	99	3.85e-1
120	4.35e-7	2.52e-8	59	1.
180	5.43e-7	1.41e-8	46	9.73e-1
240	9.48e-8	1.26e-8	38	1.40e-1
300	1.80e-8	2.28e-9	34	2.38e-2
360	1.24e-7	8.66e-9	27	1.30e-2
420	4.89e-9	9.33e-10	27	5.13e-3
480	1.55e-8	1.50e-9	26	1.57e-2
540	1.81e-9	5.34e-10	25	1.76e-3
600	4.97e-9	6.22e-10	23	4.45e-3
660	4.57e-10	1.35e-10	22	3.91e-4
720	1.70e-7	1.08e-8	22	1.46e-1
1440	2.00e-8	1.26e-9	15	1.17e-2
2880	2.75e-9	1.72e-10	11	1.18e-3

Table 7: Ripple Amplitudes (max) and half-widths for Injection and Collision Energies

The study included 3 cases consisting of one without ripple and without synchrotron oscillations, one without ripple but with synchrotron oscillations and one with ripple and with synchrotron oscillations. The ripple amplitude was increased by a factor of 10 over the values shown in Table 7 in order to produce an observable effect.

Figure 16 shows the emittances of a very fat beam as smaller than the simulated beam by a factor of approximately 6. This was also done to exaggerate the effect and make it observable. It can be seen from figure 16 that there is a barely observable emittance growth after 50,000 turns for the exaggerated simulation case. The present simulation used 256 particles in the Mar_31_lattice.

The difficulties associated with simulating the effect of power supply ripple demonstrate one of the most difficult aspects of simulating the SSC collider operation, namely the accumulation of very small errors (of the order of 1 part in 10^9) over many turns (order of 10^8). The magnitude of the physical effect is just 4 orders of magnitude larger than round-off error and hence 10^8 turns would be the absolute maximum number of turns possible to simulate assuming that errors accumulate like the square root of the number of turns. In addition to round off errors, one must consider the effect of numerical errors which could have a value greater than the ripple current as well

as other physical effects of comparable magnitude being left out of the simulation.

TC_Mar_31, Injection, Vertical

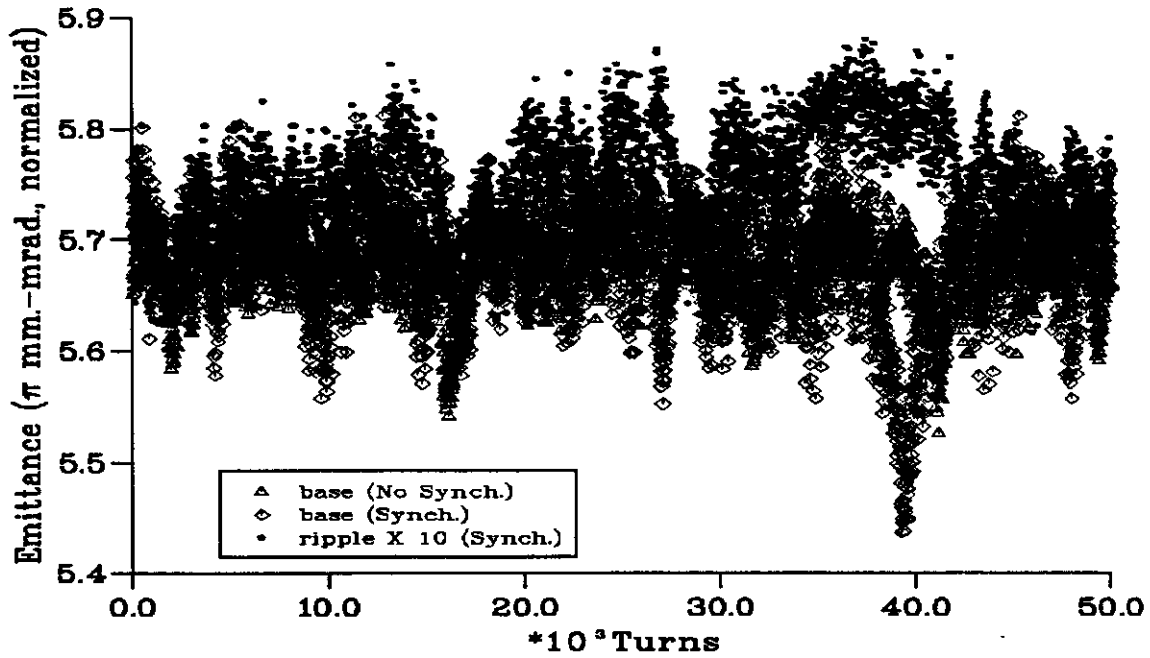


Fig. 16a Emittance growth due to power supply ripple

TC_Mar_31, Injection, Horizontal

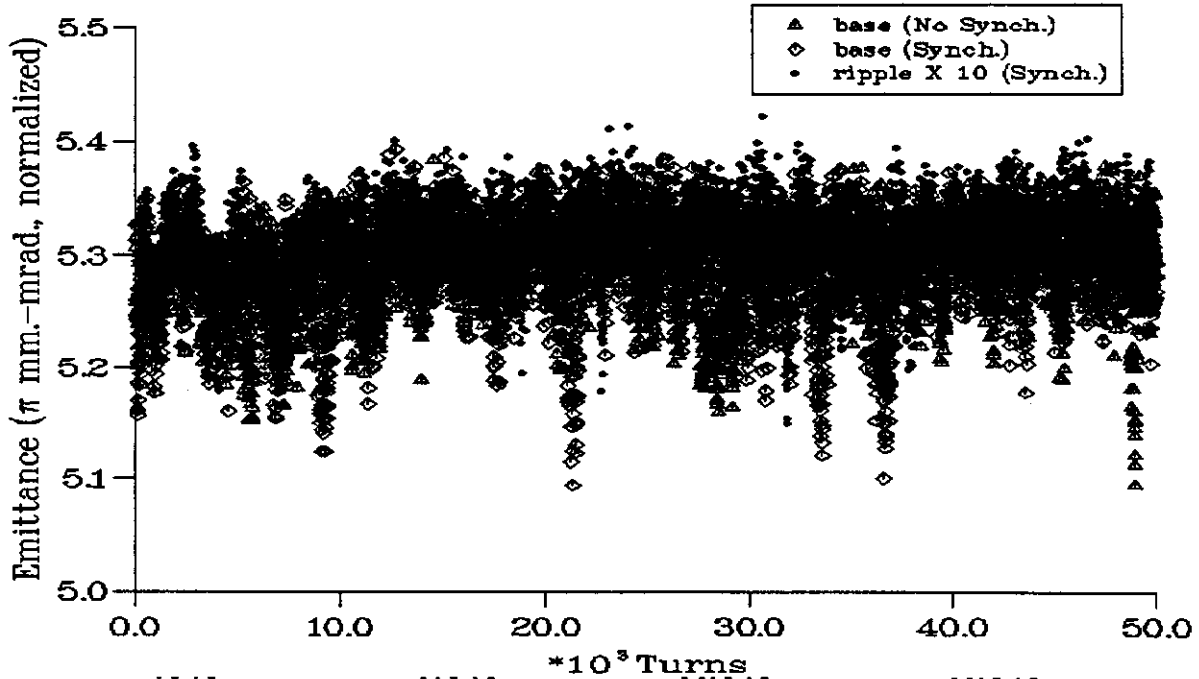


Fig 16b Emittance growth due to power supply ripple

Based on these considerations, it must be concluded that a direct simulation of the emittance blowup due to power supply ripple is beyond the capabilities of present day general simulation codes and computers. The most fruitful numerical approach appears to be write a special purpose code to analyze this effect in the absence of all others.

Advanced Techniques

The discussion above illustrates one of the limits to tracking codes. A more common limit is imposed by the CPU time and elapsed time required to calculate a given result. Using a widely accepted element by element tracking code such as TEAPOT on a large lattice such as the SSC collider will require 15 hours of CPU time on a large mainframe supercomputer to track a reasonable number of particles for 100,000 turns. One such run will typically require a week to complete in a timeshare environment. It is very desirable to be able to perform many such runs with a much quicker turn around time. Hence new hardware and software methods must be pursued to accomplish this.

SPACE CHARGE CODE

A decision was made in 1990 to apply the power of Massively Parallel Processing to the applications discussed here. To this end, the SSC acquired a 64 node ISPC/860 distributed memory parallel computer manufactured by Intel. The basic experience and performance of this machine for particle tracking without space charge effects is contained in reference 7. The principle result is that the tracking calculation can be done at approximately 10 double precision MFOPS per node at very high parallel efficiency for a rate slightly faster than a Cray YMP if all 64 nodes are used in one calculation.

The basic tracking code has been combined with an electrostatic particle in cell module to include the space charge effects in a self consistent manner. This represents a substantial extension to the physical domain of the problem. The physical model and some tracking results for the LEB is described in reference 8.

The implementation of the space charge algorithm in a distributed memory processor is considerably more difficult than the implementation of the basic tracking routines since the treatment of collective effects necessitates a great deal more inter node communication than the case of non-interacting particles. The space charge tracking code has been successfully written and tested on the parallel processor and is described in reference 9.

The execution of the space charge code is very time consuming for several reasons. One reason is that many particles must be tracked in order to produce acceptable fluctuation levels in the electrostatic field calculation. A second reason is that the space charge calculation must be done at intervals that are determined by numerical stability requirements of the PIC solver. These intervals turn out to be considerably less than the inter element spacing for the LEB and for planned beam intensities. A third reason for slower execution is that there are simply many more calculations to do. The forgoing considerations apply to any computer, serial or parallel. An additional consideration for distributed memory parallel machines is that the space charge code requires a great deal more internode communication than the non interacting particle code. Although an exact comparison is difficult, the existing implementation of the space charge code is approximately a factor of 10 slower than the non interacting particle version. This implementation of the space charge code achieves a parallel efficiency of 50 to 60 percent on 32 nodes which is

similar to efficiencies obtained in fluid dynamic calculations and other applications involving the solution of partial differential equations.

PARTICLE VISUALIZATION SYSTEM

The primary new development related to parallel processing is a high performance, interactive graphical interface known as the particle visualization system (PVS). This system can be operated synchronously with the space charge simulation so that it is possible to step the simulation time step by time step or element by element displaying the results at each iteration. The PVS is written for a Silicon Graphics Crimson workstation in C++. The control panel of the PVS is shown in figure 17.

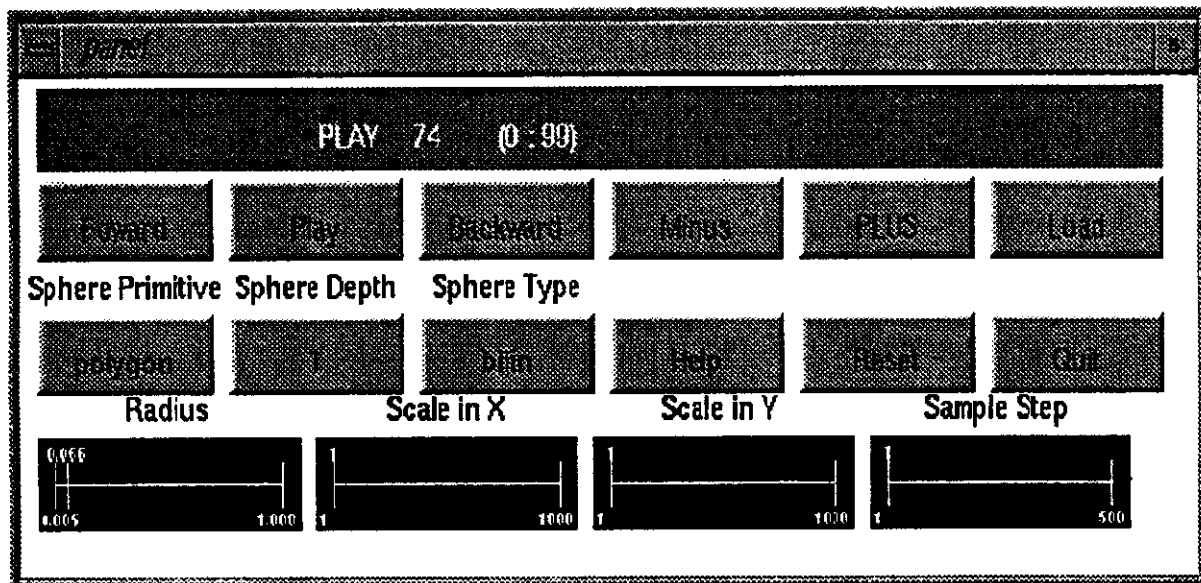


Figure 17 Control panel for Particle Visualization System

The button marked PLUS will advance the simulation and display one frame whereas the button marked minus will cause only the display to backup one frame. The button marked forward cause the simulation to proceed at its fastest rate until the end of file is encountered. Various parameters of the display can be adjusted from the slider bars at the bottom of the control panel.

The PVS can display several windows simultaneously giving different viewpoints. Figure 18 shows the particles bunch viewed from inside and outside the ring. Within each window, the viewpoint orientation and zoom range can be adjusted with the mouse. In addition, it is possible to select a viewing frame that is stationary with respect to the ring, translating with the bunch or rotating at a specified rate with respect to either of the above reference frames. There are also several options for how much of the beamline is displayed along with the particle bunch. Figure 19 shows an interior view of the bunch internal to the LEB with and without beamline elements. In either case, the inset window giving detailed specifications of the magnetic element trough which the particle is tracking can be displayed. The amount of information displayed in a given frame determines the speed at which displays can be generated and can be adjusted to the needs of the particular simulation.

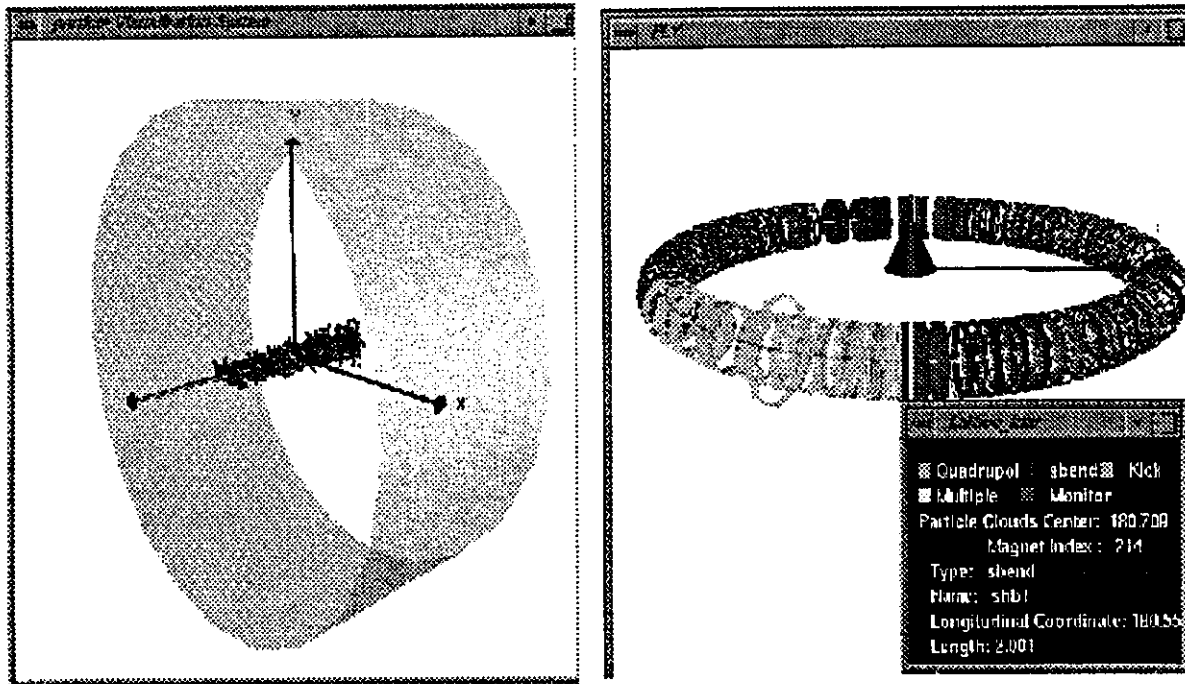


Figure 18. Exterior Views of a bunch in the LEB

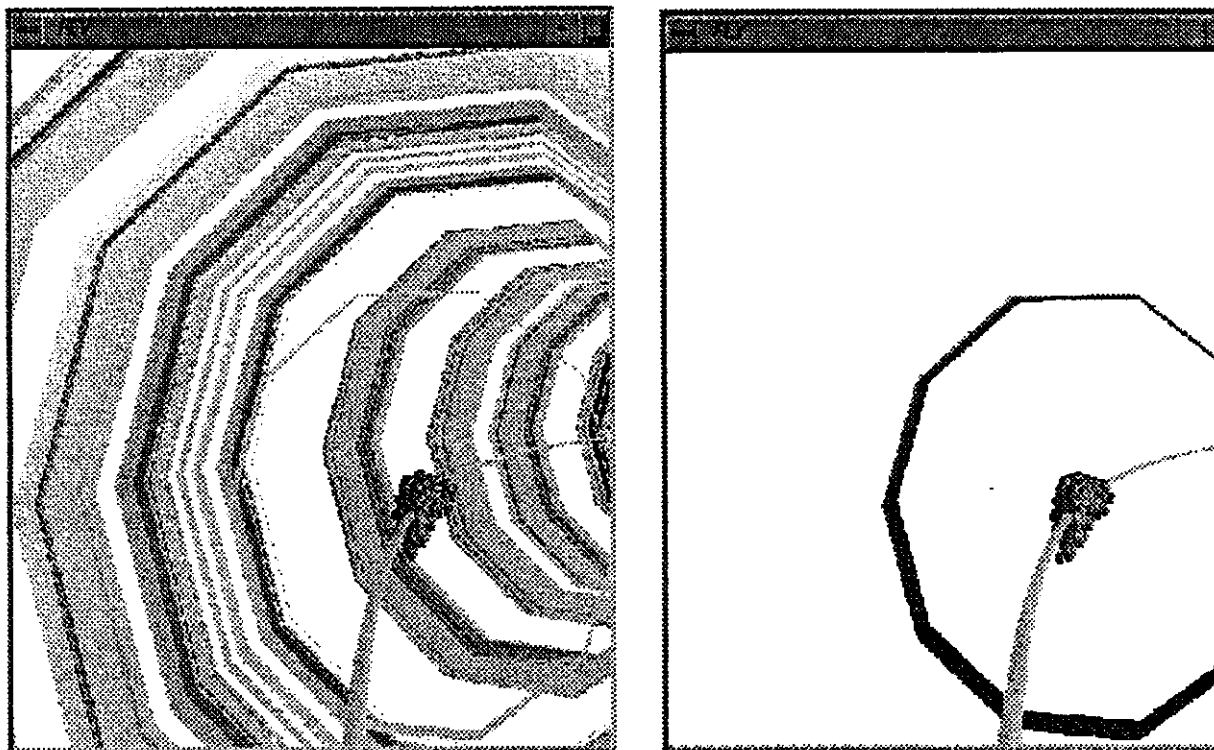


Figure 19. Interior Views of a particle bunch in the LEB

Acknowledgments

The author would specifically like to acknowledge the contributions of the following people for the pieces of work indicated. Fulvia Pilat was responsible for the simulations of local chromaticity correction in the IR's and for analyzing the effects of b_5 and b_9 errors in the triplet quadrupoles. Xiaofeng Fang was primarily responsible for the work on corrector failures. Ben Cole provided the work on emittance growth caused by power supply ripple. Long Chang did the work on the particle visualization system. Richard Talman provided many helpful insights and suggestions.

The author would like to acknowledge the support of the Defense Advanced Research Projects Agency. Some of the support was a joint DARPA/DOE program in the area of high performance computing.

The SSCL is operated by Universities Research Association, Inc., for the U.S. Department of Energy under Contract No. DE-AC35-89ER40486

References

1. Y. Noschokov, F. Pilat, T. Sen, Chromaticity Correction for the Collider at the SSC, *This Proceeding*.
2. R. Talman, Single Particle Motion, *Notes for joint US-CERN school on Beam Observation, Diagnosis and Correction*, Capri, Italy, 1988.
3. G. Bourianoff, S. Hunt, D. Mathieson, F. Pilat, R. Talman, G. Morpurgo, Determination of Coupled-Lattice Properties Using Turn-By-Turn Data.-SSCL Preprint#181, Dec. 1992
4. A. M. Fauchet, T. Fieguth, J. P. Koutchouk, T. Risselada, Coupling in LEP(II): Azimuthal Distribution in Octants 2,3 & 4, *LEP Commissioning Note 18*, Dec. 1989.
5. L. Schachinger and R. Talman, Teapot: Thin-Element Accelerator Program for Optics and Tracking, *Particle Accelerators*, 1987, Vol. 22, pp. 35-56.
6. D. Bintinger et. al., *The Compensation of SSC lattice Optics in the Presence of Dipole Field Errors*, SSC-SR-1038, Feb, 1989, p. 11.
7. G. Bourianoff and B. Cole, Parallel Processing at the SSC: The Fact and the Fiction, *Advanced Beam Dynamics Workshop on Effects of Errors in Accelerators, Their Diagnoses and Corrections*, AIP Conference Proceedings No. 255, Corpus Christi, Texas, 1991.
8. S. Machida, G. Bourianoff, Y. Huang and N. K. Mahale, "Tracking Study of Hadron Boosters", *XV International Conference on High Energy Accelerators*, 1992, Hamburg, Germany.
9. L.C. Chang, G. Bourianoff, B. Cole and S. Machida, "A parallel Implementation of Particle Tracking with Space Charge Effects on an Intel IPSC/860, SSCL